

A label-free sub-diffractive technique for 3D intracellular tomography using thermally induced convection currents

Jayesh Goswami,^{†,§} Shataneek Banerjee,^{†,§} Snigdhadev Chakraborty,[†] Srestha Roy,[†] Atanu Ghosh,[†] Mrutyunjaya Rath,[†] Agniva Das,[†] Mukul Sagar,[†] Krishna Kumari Swain,[†] Prasanta Pal,[‡] and Basudev Roy^{*,¶}

[†]*Department of Physics, Quantum Centre of Excellence for Diamond and Emergent Materials (QuCenDiEM), IIT Madras, Chennai 600036, India*

[‡]*SHIOM LLC, Westborough, Massachusetts, USA, and RIHUB, Rhode Island, USA*

[¶]*Department of Chemistry, Unknown University, Unknown Town*

[§]*Equal contribution*

E-mail: basudev@iitm.ac.in

Abstract

Conventionally, 3-dimensional cellular tomography can be done with light sheet or multi-angle observations. Recently, a new technique was introduced where the cell was rotated using convection currents to visualize the outer periphery (Liu et al., Nano Lett., 2023, 23, 5148). However, the work falls short of actually observing intracellular objects like organelles etc. In this manuscript, we modify the technique by relying on computer vision algorithm called Contrast Limited Adaptive Histogram Equalisation (CLAHE) to improve the contrast for better detection of intra-cellular points, and then use optical flow detection technique to extract the in-plane speed of the point. This

then is used to extract the vertical location, knowing that at the bottom part of the sphere, the point would be moving in one direction, close to the center there would be much less motion, while in the top portion of the sphere, the point would be moving in the reverse direction than the bottom. The velocity allows the exact localisation of the point in the vertical direction. This process allows for sub-diffractive intracellular tomography. This technique can further allow high-resolution detection of fluorescent molecules inside the cell also, when combined with convective flows.

Introduction

The study and analysis of the three-dimensional (3D) characteristics of cells and organisms are of fundamental importance for understanding the structure and network.^{1,2} Conventionally, cellular imaging is done by taking multiple sequential images of a two-dimensional (2D) focal plane to form a focal stack. This technique gives high resolution along the lateral axis (x-axis), but leads to low resolution and missing information along the other axis, which is insufficient to visualize and resolve subcellular phenomena.³⁻⁵ Other methods include total internal reflection fluorescence⁶⁻¹⁰ and selective plane illumination microscopy (SPIM)¹¹⁻¹⁶ but this technique focuses on only a small portion of the sample close to the objective for high-resolution imaging.^{17,18}

Recently, multiview SPIM has also been introduced by adding multiple objective to scan the sample through multiple directions to overcome the detrimental effects of occlusion, scattering, and optical shadowing and improve the overall 3D imaging.^{19,20} However, this technique also cannot provide full 360° optical imaging with high resolution.²¹ In another technique, rotating the sample continuously can provide a full 360° optical imaging even with standard optical microscope,^{22,23} by rotating the sample the missing information of the shadowing region can be captured. Thus, it can provide high-resolution imaging. However, this technique requires a fixed sample configuration on the substrate for stability and precision.¹⁷ The alternative way includes using external fields(i.e., optical, acoustic, and magnetic) for

rotation. few such setups include optical and magnetic tweezers, the inclusion of these external field-based manipulation techniques is very helpful in various experiments to give best results as they are noncontact, compatible with biological samples, and easy to integrate with microfluidic devices.^{24,25}

Optical tweezers have been proven to provide precise control and generate good results in experiments involving cell size ranging from nanoscales to microscales. it can trap and can provide tomographic properties down to single-molecule level.^{26,27} optical tweezers uses tightly focused laser beams for trapping and performing 3D manipulation of micro-particles, cells, and proteins.²⁸⁻³² However, achieving stable rotation with conventional optical tweezers is difficult due to the high mobility and asymmetry nature of the particles, which results in missing information and inaccurate optical imaging.^{33,34} However, recent work reported that hydrodynamic flows provided an excellent and stable particle rotation.³⁵⁻⁴⁰

In this work we try to generate the cell rotation using thermophoretic flows. We create a sample chamber using a Dictyostelium cells as a sample, and putting them on gold-coated cover slip. As we direct the laser beam on the gold surface, it gets heated up and generates convection currents, which in turn lead to thermophoretic flows, inducing rotation of the cells. We extract the frames from the video of cell rotation. After extracting the frames, the contrast of each frame is enhanced using Contrast Limited Adaptive Histogram Equalization (CLAHE). The cell of interest is segmented out from the contrast enhanced frames. A number of intra-cellular points have been tracked from one frame to a subsequent one using Lucas Kanade Optical Flow. Finally the radial distance of those tracked points have been computed using a geometry-based method using properties of circle. The points plotted at the corresponding radial distances yields the three dimensional reconstruction of the cell.

Theoretical details

We generate the convection currents by using a recently developed technique, where we first make a sample chamber with the bottom surface having a layer of gold on it. Then we illuminate a laser beam from the bottom objective into the bottom gold surface that induces convection currents close to the bottom surface. These convection currents then rotate the cell in the out of plane sense,^{21,41} as shown in Fig. 1 (a).

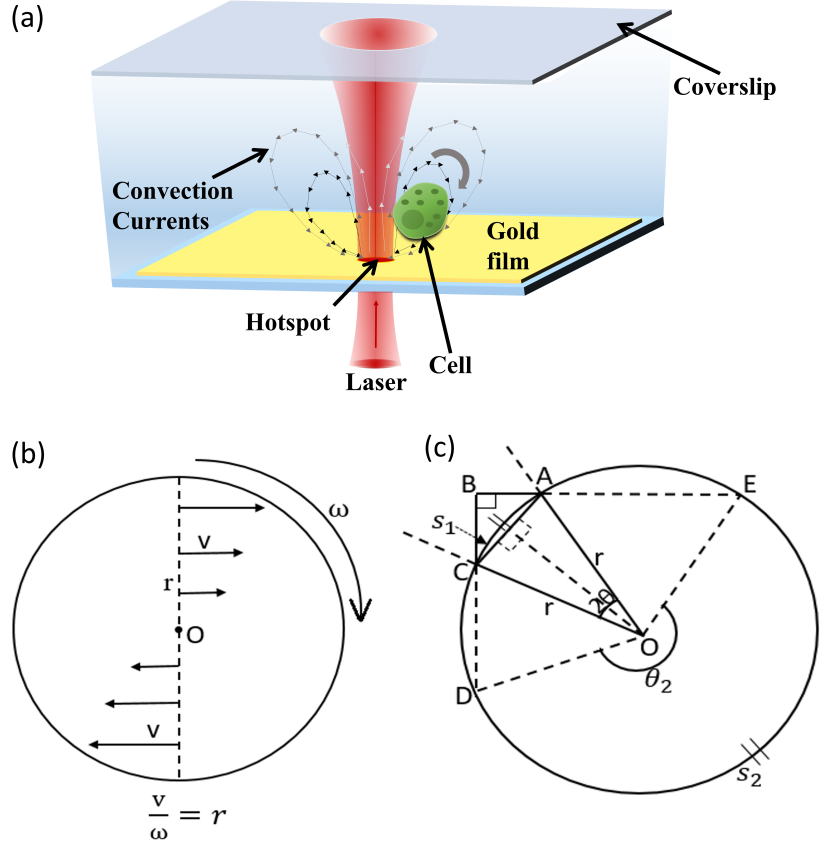


Figure 1: This figure shows the cell rotation mechanism and geometrical analysis (a) shows the cell rotation under the influence of convection current generated by the heating of gold film. (b) shows Intra-cellular velocity profile along the central line. (c) shows Calculation of radial distance of intra-cellular points.

Once the cell rotates, the points inside the cell are made distinctly visible by enhancing the contrast using CLAHE and then their motion tracked. We extract the coordinates of the points, particularly the z location by a method shown in Fig. 1 (b). Once the cell rotates, the outer points move with a velocity higher than the points towards the middle. Then towards the bottom, the points move reverse to the the motion at the top. However, in all of the cases of the points, the angular velocity is constant. This facet is used to first determine the angular velocity and then, from the velocity vectors, extract the depth at which the particle is located, as shown in Fig. 1(b) and (c).

In this work, we have tried to perform a 3D reconstruction of a single cell interior using the technique mentioned. We have used Dictyostelium cells for our study. A typical event where the cell is rotated using the heated gold substrate has been shown in Fig. 2, taken with a phase contrast microscope at a very high Numerical Aperture (N.A.) of 1.49. This automatically assists in visualisation of sub-diffractive objects till about 100 nm or so.

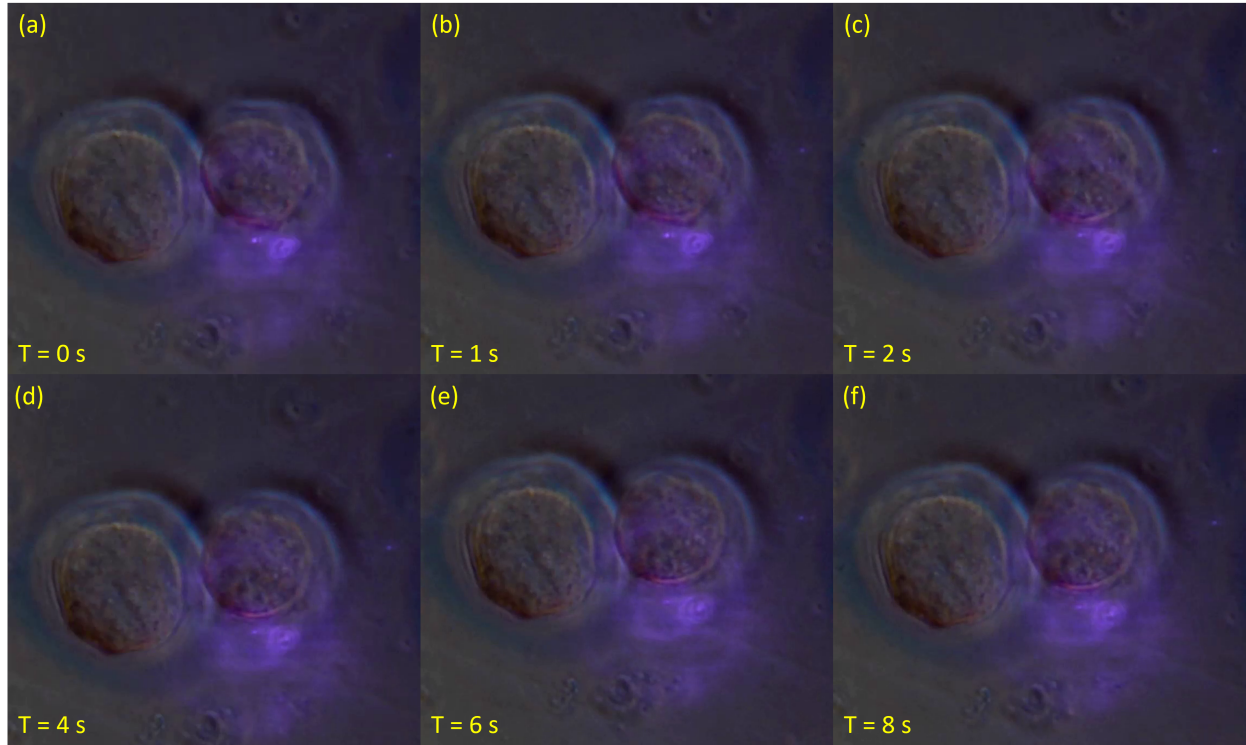


Figure 2: The figure shows the collage of different snapshots of cell taken at different time interval.

Contrast enhancement of images

Different time snapshots inside the video have been enhanced using the Contrast Limited Adaptive Histogram Equalization (CLAHE) algorithm to facilitate efficient detection of salient points within the cell. The image was divided into different sub-sections and a histogram (Fig. 3c) was computed for each sub-section.⁴² Then the pixel values were adjusted to increase the flatness of the histogram (Fig. 3d). The way this was performed was to increase the grayscale value of the pixels which are less frequent, while also decreasing the grayscale value of the pixels which have high frequency in the histogram. This increase in flatness of the histogram leads to improvement of the image contrast and makes the points more distinctly visible.⁴³

The following equation demonstrates the application of CLAHE to an image⁴⁴ :

$$I'(x, y) = \sum_{i=1}^N w_i \cdot T_i(I(x, y)) \quad (1)$$

where:

$I(x, y)$ is the input pixel intensity at the location (x, y)

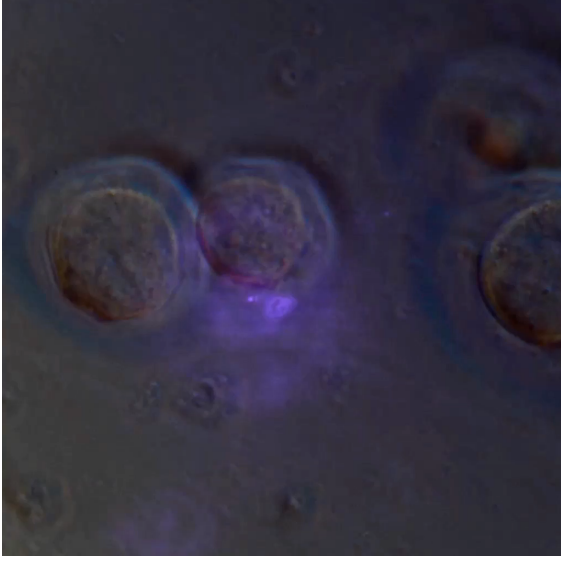
$I'(x, y)$ is the output pixel intensity at the location (x, y)

$T_i(I(x, y))$ is the transformation function for the i -th neighboring tile

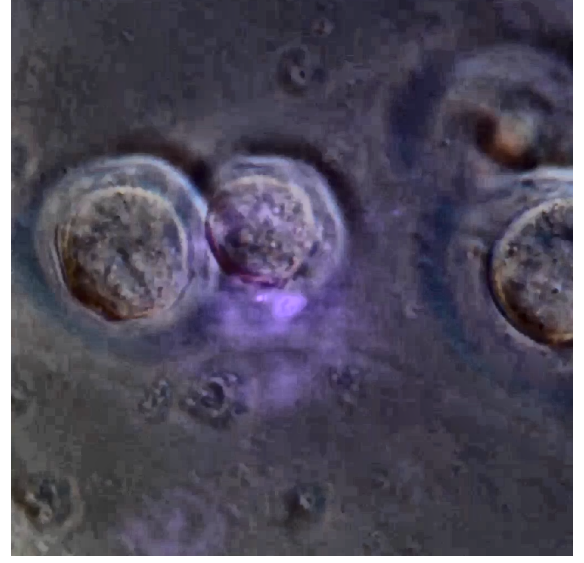
w_i are bilinear interpolation weights

An example application of CLAHE to one snapshot of the video has been shown in Figure

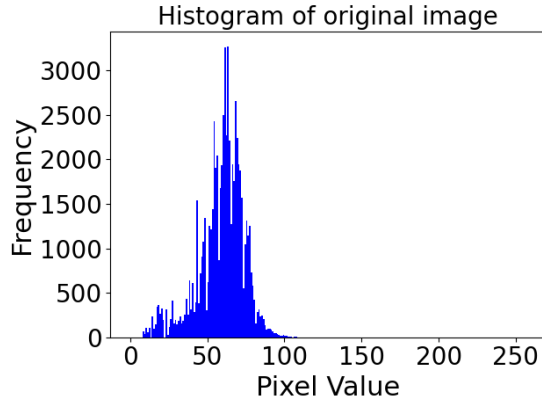
3.



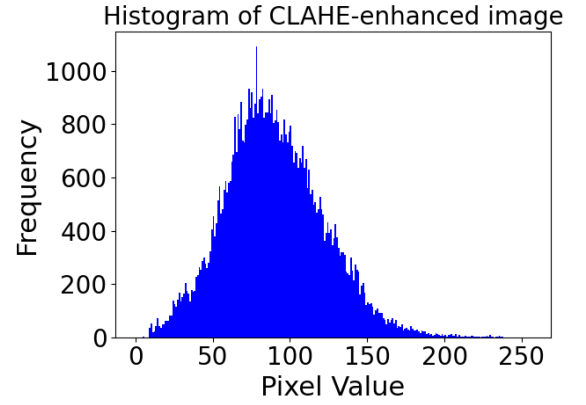
(a) One snapshot of the video



(b) Contrast enhanced image



(c) Histogram of original image



(d) Histogram of contrast enhanced image.

Figure 3: Application of CLAHE to images. Here we have increased the grayscale value of the pixels which are less frequent, while also decreasing the grayscale value of the pixels which have high frequency in the histogram

Calculation of radial distance of different intra-cellular points

After the initial and final position of points have been tracked using optical flow, the radial distance of the points are calculated using a mathematical formulation that is based on rotational dynamics of spherical bodies. The equations to be solved have been listed below:

$$v = \omega \times r \quad (2)$$

$$\frac{BC}{BD} = \frac{\sin(\theta)}{\sin(\theta_2/2)} \quad (3)$$

$$\frac{s_2 - s_1}{r} = \pi \quad (4)$$

$$CD = 2r \cos\left(\frac{\theta_2}{4} + \frac{\theta}{2}\right) \quad (5)$$

The notations used in the equations are based on Figure 1(b) and (c). Solving the above equations for each point within the cell gives its corresponding radial distance.

Point tracking using optical flow

The cell of interest is segmented out from different snapshots of the video. Lucas Kanade (L-K) optical flow algorithm is applied on the segmented cell at two different time frames. L-K method is a widely used optical flow estimation method that uses the least squares criterion to solve the optical flow equations in a local neighborhood of a particular pixel.

L-K method solve the following system of equations:⁴⁵

$$A^T A v = A^T b \quad (6)$$

where:

$$A = \begin{bmatrix} I_x(q_1) & I_y(q_1) \\ I_x(q_2) & I_y(q_2) \\ \vdots & \vdots \\ I_x(q_n) & I_y(q_n) \end{bmatrix} \quad v = \begin{bmatrix} V_x \\ V_y \end{bmatrix} \quad b = \begin{bmatrix} -I_t(q_1) \\ -I_t(q_2) \\ \vdots \\ -I_t(q_n) \end{bmatrix}$$

Optical flow estimation gives the positional shift of different spatial points inside the cell

between the two time frames as shown in Figure 4. The coordinates of the points in the two frames are tabulated in Table 1. The velocities of the points at the top and bottom of the cell are opposite in direction as demonstrated in the velocity profile shown in Figure 1.

Table 1: Coordinates of different points in the earlier and later frames

Point No.	Earlier Time Frame		Later Time Frame	
	x coordinate (pixels)	y coordinate (pixels)	x coordinate (pixels)	y coordinate (pixels)
1	455.9	416.2	455.0	419.1
2	467.0	404.5	466.6	408.7
3	487.7	408.0	488.9	413.6
4	477.1	415.9	476.8	420.3
5	473.8	456.2	475.0	464.5
6	434.3	447.9	435.2	455.2
7	453.0	449.7	453.9	456.6
8	487.7	457.9	489.1	466.1
9	497.1	470.2	498.2	476.5
10	502.7	415.1	504.2	419.7
11	415.4	397.3	412.3	397.1
12	426.5	407.8	421.6	404.3
13	398.7	428.7	397.3	428.5
14	445.0	347.2	439.9	346.2
15	392.3	438.0	390.9	437.7

The fact that the minimum resolution of these coordinates is about 0.1 pixels, means that the resolution of detection of these points is about 10 nm, given that each pixels corresponds to about 100 nm. The localisation accuracy was further enhanced by enhancing the distinctiveness of the points using CLAHE.

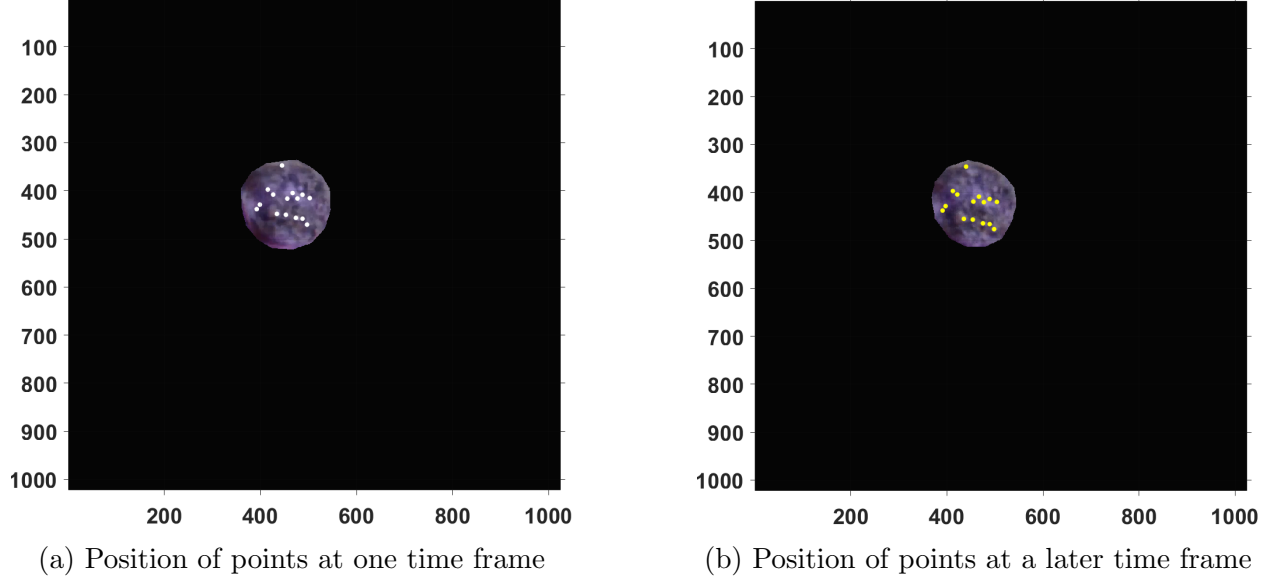


Figure 4: Point tracking by optical flow

Sample preparation

Dictyostelium cells (wild-type *D. discoideum* AX2) were prepared by inoculating spores into 90 mm tissue culture plates filled with axenic HL5 growth medium (HLG01XX – Formedium, Norfolk, UK, pH 6.4), supplemented with streptomycin sulfate (100 mg/ml) and penicillin (100 units per ml). The cultures were incubated at 22 °C until they became semi-confluent. Cells in the mid-log phase were harvested in ice cold KK2 buffer (2.2 g/l KH₂ PO₄ and 0.7 g/l K₂ HPO₄, pH 6.4), washed twice and 5×10^6 cells were pelleted and placed in ice for performing further tests.

Experimental details

The experiment uses an inverted microscope (Nikon Eclipse Ti2E) integrated with an optical tweezers setup, equipped with a 60 \times , oil-immersion type objective lens with 1.49 Numerical aperture (N.A.) for simultaneous imaging and trapping. The condenser used was CLWD 10 \times with 0.72 N.A. (air-immersion) from Nikon. A 1064 nm wavelength solid state laser (Opus

1064) was employed for the experiment. The schematic representation of the experimental setup is depicted in Fig.5.

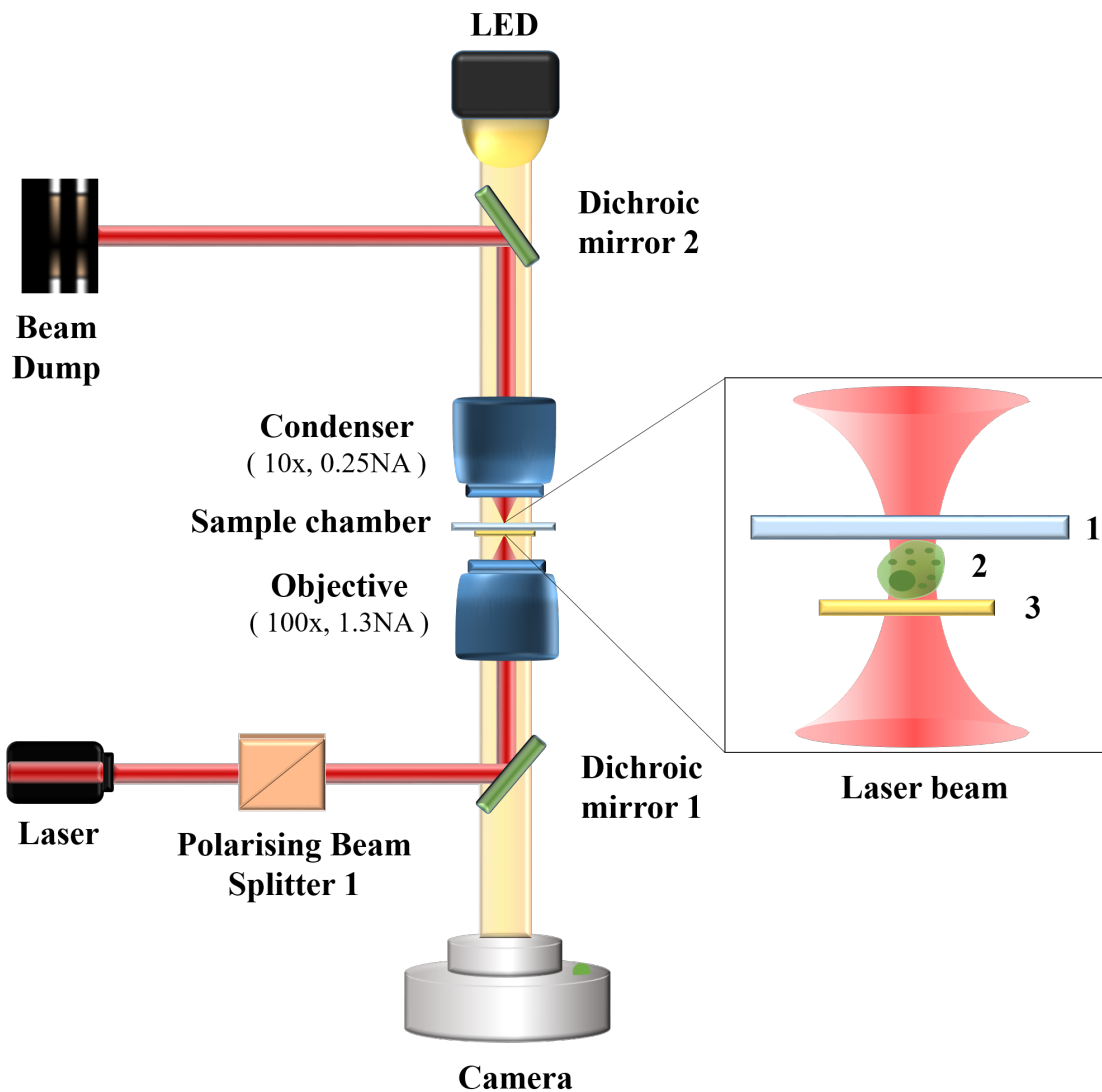


Figure 5: The schematic diagram of the experimental setup is shown (1) Glass slide (2) Dictyostelium cells (3) Gold coverslip

The samples utilized in these experiments were Dictyostelium cells whose detailed preparation procedure is mentioned in the sample preparation section. A 20 μL aliquot of the sample was carefully placed on a glass slide (Blue star, number 1 size, English glass), then a gold-coated coverslip, (Blue star, number 1 size, English glass) of thickness 160 μm with

a 30 nm gold coating layer, was placed over the aqueous dispersion to complete the sample chamber. The prepared sample chamber was positioned on the sample stage of the optical tweezers setup, in an inverted position. A white light LED source is used to illuminate the sample stage. The output is collected by a CMOS camera placed at the output port for imaging purposes, as shown in Fig.1. The sample chamber was irradiated with a 1064nm laser beam, originating from the bottom of the chamber. Due to the plasmonic properties of gold, the regions where the laser beams interact with the gold-coated surface experience substantial heating, which in turn leads to an increase in the temperature of the surrounding medium, thereby inducing convection currents within the aqueous dispersion of cells. The temperature of the room was maintained at 25°C using an air conditioner.

Results and Discussions

The 3-D map of the points inside the cell are made and the results depicted in Fig. 6. The location of the objects inside the cell have been indicated from two different projections, and a bright field image shown for comparison. The points shown in the projections may have moved somewhat in the brightfield image, being from a different frame. It can be noticed that the resolution available for detecting these objects is limited by the resolution of detection of the x and y coordinates of the center of the spot. This is typically of the order of 10 nm. Thus, the resolution of detection of the z coordinate is also of that order and hence sub-diffractive. This bypasses the main problem in previous attempts where the spots could not be detected.

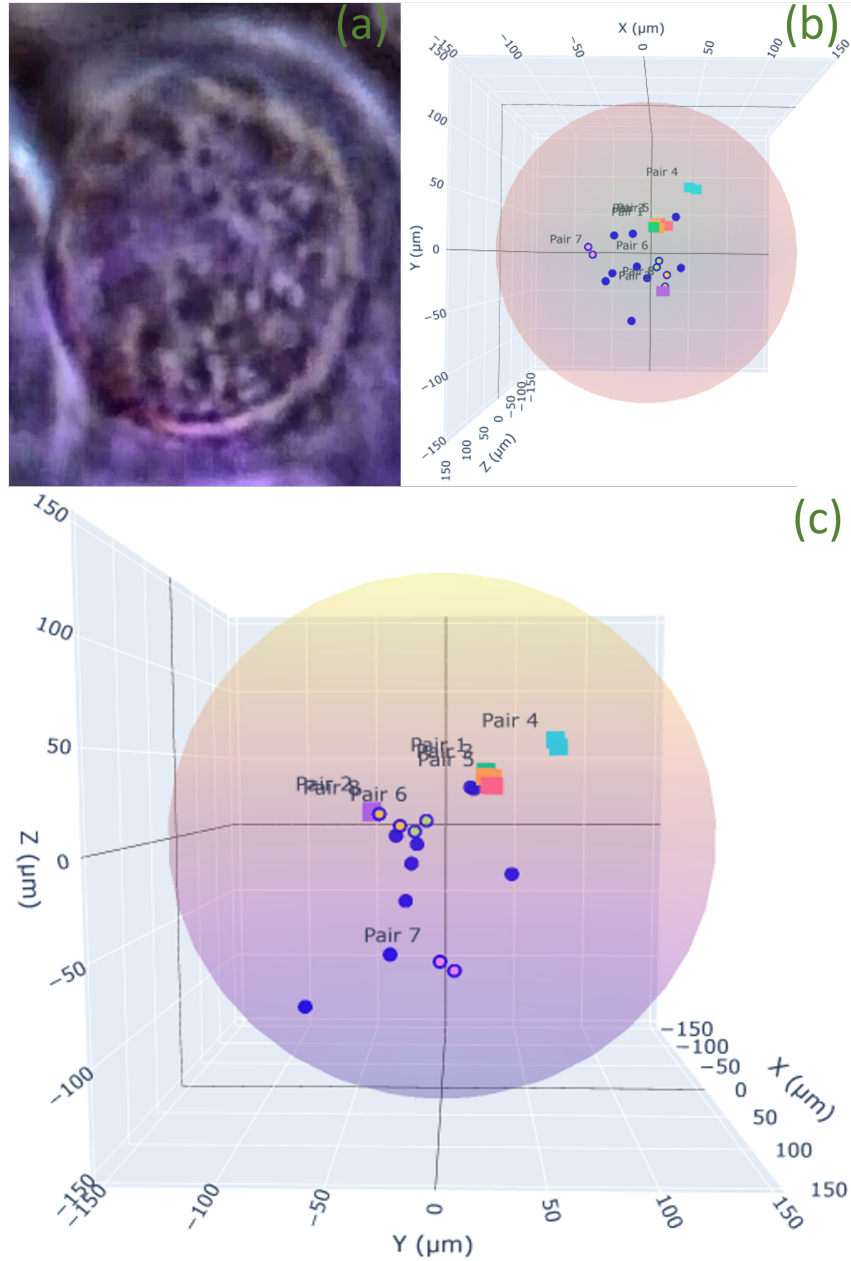


Figure 6: (a) Live cell image after significant contrast improvement, looked at from the top. (b) top view (c) front view The (a) and (b) may be different time points of the same event, but (b) and (c) correspond to same time point.

In this manuscript, we use computer vision techniques to detect and track such objects inside the cell. Instead of just visualising the cell from different angles, we use a trick to locate the particles relying upon their speeds of motion, that allows sub-diffractive localisation of these.

Conclusions

Thus, to conclude, we report a new technique to perform 3D intracellular tomography by rotating the cell partially and then use the velocity of the intracellular points as a signature of the depth of the particle. The method does not require complete 360 degree rotation of the cell, like used earlier, and yet performs the job of the tomography. The points are detected by using computer vision technique called CLAHE algorithm which is very good at extracting signals from noise and then using the optical flow detection technique to track the point over multiple frames. The method would assist conventional methods to detect even single fluorescent or label-free⁴⁶ scattering objects to ascertain the vertical location of the point to sub-diffractive resolution of about 10 nm.

Conflict of Interest

The authors declare that they have no known competing financial interests or personal relationships that could have appeared to influence the work reported in this paper. P.P. has co-founded a company, SHIOM LLC to commercialize technologies involving improvement in signal of noise of images.

Acknowledgement

We thank the Indian Institute of Technology, Madras, India, for their seed and initiation grants to Basudev Roy. This work was also supported by the DBT/Wellcome Trust India Alliance Fellowship IA/I/20/1/504900 awarded to Basudev Roy.

References

- (1) Monks, C. R.; Freiberg, B. A.; Kupfer, H.; Sciaky, N.; Kupfer, A. Three-dimensional segregation of supramolecular activation clusters in T cells. *Nature* **1998**, *395*, 82–86.
- (2) Wu, W.; Singh, M.; Masud, A.; Wang, X.; Nallapaneni, A.; Xiao, Z.; Zhai, Y.; Wang, Z.; Terlier, T.; Bleuel, M.; others Control of phase morphology of binary polymer grafted nanoparticle blend films via direct immersion annealing. *ACS nano* **2021**, *15*, 12042–12056.
- (3) Swoger, J.; Verveer, P.; Greger, K.; Huisken, J.; Stelzer, E. H. Multi-view image fusion improves resolution in three-dimensional microscopy. *Optics express* **2007**, *15*, 8029–8042.
- (4) Lidke, D. S.; Lidke, K. A. Advances in high-resolution imaging–techniques for three-dimensional imaging of cellular structures. *Journal of cell science* **2012**, *125*, 2571–2580.
- (5) Li, B.; Tan, S.; Dong, J.; Lian, X.; Zhang, Y.; Ji, X.; Veeraraghavan, A. Deep-3D microscope: 3D volumetric microscopy of thick scattering samples using a wide-field microscope and machine learning. *Biomedical Optics Express* **2021**, *13*, 284–299.
- (6) Mattheyses, A. L.; Simon, S. M.; Rappoport, J. Z. Imaging with total internal reflection fluorescence microscopy for the cell biologist. *Journal of cell science* **2010**, *123*, 3621–3628.
- (7) Axelrod, D.; Thompson, N. L.; Burghardt, T. P. Total internal reflection fluorescent microscopy. *Journal of microscopy* **1983**, *129*, 19–28.
- (8) Fish, K. N. Total internal reflection fluorescence (TIRF) microscopy. *Current protocols in cytometry* **2009**, *50*, 12–18.
- (9) Chung, E.; Kim, D.; Cui, Y.; Kim, Y.-H.; So, P. T. Two-dimensional standing wave total

- internal reflection fluorescence microscopy: superresolution imaging of single molecular and biological specimens. *Biophysical journal* **2007**, *93*, 1747–1757.
- (10) Sako, Y.; Uyemura, T. Total internal reflection fluorescence microscopy for single-molecule imaging in living cells. *Cell structure and function* **2002**, *27*, 357–365.
 - (11) Huiskens, J.; Swoger, J.; Del Bene, F.; Wittbrodt, J.; Stelzer, E. H. Optical sectioning deep inside live embryos by selective plane illumination microscopy. *Science* **2004**, *305*, 1007–1009.
 - (12) Huiskens, J.; Stainier, D. Y. Selective plane illumination microscopy techniques in developmental biology. **2009**,
 - (13) Fu, Q.; Martin, B. L.; Matus, D. Q.; Gao, L. Imaging multicellular specimens with real-time optimized tiling light-sheet selective plane illumination microscopy. *Nature communications* **2016**, *7*, 11088.
 - (14) Gao, L. Optimization of the excitation light sheet in selective plane illumination microscopy. *Biomedical optics express* **2015**, *6*, 881–890.
 - (15) Hedde, P. N.; Ranjit, S.; Gratton, E. 3D fluorescence anisotropy imaging using selective plane illumination microscopy. *Optics Express* **2015**, *23*, 22308–22317.
 - (16) Huiskens, J.; Stainier, D. Y. Even fluorescence excitation by multidirectional selective plane illumination microscopy (mSPIM). *Optics letters* **2007**, *32*, 2608–2610.
 - (17) Axelrod, D. Total internal reflection fluorescence microscopy in cell biology. *Traffic* **2001**, *2*, 764–774.
 - (18) Power, R. M.; Huiskens, J. A guide to light-sheet fluorescence microscopy for multiscale imaging. *Nature methods* **2017**, *14*, 360–373.
 - (19) He, J.; Huiskens, J. Image quality guided smart rotation improves coverage in microscopy. *Nature communications* **2020**, *11*, 150.

- (20) Chang, B.-J.; Manton, J. D.; Sapoznik, E.; Pohlkamp, T.; Terrones, T. S.; Welf, E. S.; Murali, V. S.; Roudot, P.; Hake, K.; Whitehead, L.; others Real-time multi-angle projection imaging of biological dynamics. *Nature methods* **2021**, *18*, 829–834.
- (21) Liu, Y.; Unni, R.; Lou, X.; Yang, M.; Zheng, Y. High-Resolution Volumetric Imaging and Classification of Organisms with Standard Optical Microscopy. *Nano Letters* **2023**, *23*, 5148–5154.
- (22) Calisesi, G.; Candeo, A.; Farina, A.; D’Andrea, C.; Magni, V.; Valentini, G.; Pistocchi, A.; Costa, A.; Bassi, A. Three-dimensional bright-field microscopy with isotropic resolution based on multi-view acquisition and image fusion reconstruction. *Scientific reports* **2020**, *10*, 12771.
- (23) Chhetri, R. K.; Amat, F.; Wan, Y.; Höckendorf, B.; Lemon, W. C.; Keller, P. J. Whole-animal functional and developmental imaging with isotropic spatial resolution. *Nature methods* **2015**, *12*, 1171–1178.
- (24) Ahmed, D.; Ozcelik, A.; Bojanala, N.; Nama, N.; Upadhyay, A.; Chen, Y.; Hanna-Rose, W.; Huang, T. J. Rotational manipulation of single cells and organisms using acoustic waves. *Nature communications* **2016**, *7*, 11085.
- (25) Tang, T.; Hosokawa, Y.; Hayakawa, T.; Tanaka, Y.; Li, W.; Li, M.; Yalikun, Y. Rotation of biological cells: fundamentals and applications. *Engineering* **2022**, *10*, 110–126.
- (26) Sudhakar, S.; Abdosamadi, M. K.; Jachowski, T. J.; Bugiel, M.; Jannasch, A.; Schäffer, E. Germanium nanospheres for ultraresolution picotensiometry of kinesin motors. *Science* **2021**, *371*, eabd9944.
- (27) Moffitt, J. R.; Chemla, Y. R.; Smith, S. B.; Bustamante, C. Recent advances in optical tweezers. *Annu. Rev. Biochem.* **2008**, *77*, 205–228.

- (28) Ndukaife, J. C.; Kildishev, A. V.; Nnanna, A. G. A.; Shalaev, V. M.; Wereley, S. T.; Boltasseva, A. Long-range and rapid transport of individual nano-objects by a hybrid electrothermoplasmonic nanotweezer. *Nature nanotechnology* **2016**, *11*, 53–59.
- (29) Pang, Y.; Song, H.; Kim, J. H.; Hou, X.; Cheng, W. Optical trapping of individual human immunodeficiency viruses in culture fluid reveals heterogeneity with single-molecule resolution. *Nature nanotechnology* **2014**, *9*, 624–630.
- (30) Pang, Y.; Gordon, R. Optical trapping of a single protein. *Nano letters* **2012**, *12*, 402–406.
- (31) Marago, O. M.; Jones, P. H.; Gucciardi, P. G.; Volpe, G.; Ferrari, A. C. Optical trapping and manipulation of nanostructures. *Nature nanotechnology* **2013**, *8*, 807–819.
- (32) Ashkin, A.; Dziedzic, J. M.; Yamane, T. Optical trapping and manipulation of single cells using infrared laser beams. *Nature* **1987**, *330*, 769–771.
- (33) Avsievich, T.; Zhu, R.; Popov, A.; Bykov, A.; Meglinski, I. The advancement of blood cell research by optical tweezers. *Reviews in Physics* **2020**, *5*, 100043.
- (34) Arzola, A. V.; Jákl, P.; Chvátal, L.; Zemánek, P. Rotation, oscillation and hydrodynamic synchronization of optically trapped oblate spheroidal microparticles. *Optics express* **2014**, *22*, 16207–16221.
- (35) Panja, K.; Goswami, J.; Nalupurackal, G.; Chakraborty, S.; Roy, S.; Roy, B.; Singh, R. Nonlinear dynamics of a microparticle in a hydro-thermophoretic trap. *Results in Physics* **2024**, *61*, 107709.
- (36) Nalupurackal, G.; Gunaseelan, M.; Roy, S.; Lokesh, M.; Kumar, S.; Vaippully, R.; Singh, R.; Roy, B. A hydro-thermophoretic trap for microparticles near a gold-coated substrate. *Soft matter* **2022**, *18*, 6825–6835.

- (37) Sun, J.; Koukourakis, N.; Guck, J.; Czarske, J. W. Rapid computational cell-rotation around arbitrary axes in 3D with multi-core fiber. *Biomedical Optics Express* **2021**, *12*, 3423–3437.
- (38) Jünger, F.; Ruh, D.; Strobel, D.; Michiels, R.; Huber, D.; Brandel, A.; Madl, J.; Gavrilov, A.; Mihlan, M.; Daller, C. C.; others 100 Hz ROCS microscopy correlated with fluorescence reveals cellular dynamics on different spatiotemporal scales. *Nature Communications* **2022**, *13*, 1758.
- (39) Schürmann, M.; Cojoc, G.; Girardo, S.; Ulbricht, E.; Guck, J.; Müller, P. Three-dimensional correlative single-cell imaging utilizing fluorescence and refractive index tomography. *Journal of biophotonics* **2018**, *11*, e201700145.
- (40) Nalupurackal, G.; Panja, K.; Chakraborty, S.; Roy, S.; Goswami, J.; Roy, B.; Singh, R. Controlled roll rotation of a microparticle in a hydro-thermophoretic trap. *Physical review research* **2023**, *5*, 033005.
- (41) Kumar, S.; Gunaseelan, M.; Vaippully, R.; Kumar, A.; Ajith, M.; Vaidya, G.; Dutta, S.; Roy, B. Pitch-rotational manipulation of single cells and particles using single-beam thermo-optical tweezers. *Biomedical Optics Express* **2020**, *11*, 3555–3566.
- (42) Mondal, K.; Rabidas, R.; Dasgupta, R. Single image haze removal using contrast limited adaptive histogram equalization based multiscale fusion technique. *Multimedia Tools and Applications* **2024**, *83*, 15413–15438.
- (43) Yoshimi, Y.; Mine, Y.; Ito, S.; Takeda, S.; Okazaki, S.; Nakamoto, T.; Nagasaki, T.; Kakimoto, N.; Murayama, T.; Tanimoto, K. Image preprocessing with contrast-limited adaptive histogram equalization improves the segmentation performance of deep learning for the articular disk of the temporomandibular joint on magnetic resonance images. *Oral Surgery, Oral Medicine, Oral Pathology and Oral Radiology* **2024**, *138*, 128–141.

- (44) Chen, R.-C.; Dewi, C.; Zhuang, Y.-C.; Chen, J.-K. Contrast limited adaptive histogram equalization for recognizing road marking at night based on YOLO models. *IEEE Access* **2023**, *11*, 92926–92942.
- (45) Al-Qudah, S.; Yang, M. Large displacement detection using improved lucas–kanade optical flow. *Sensors* **2023**, *23*, 3152.
- (46) Kasaian, K.; Mazaheri, M.; Sandoghdar, V. Long-Range Three-Dimensional Tracking of Nanoparticles Using Interferometric Scattering Microscopy. *ACS nano* **2024**, *18*, 30463–30472.